2D2-1

STATISTICAL ANALYSIS OF HIGH RESOLUTION SUBSURFACE IMAGES WITH APPLICATION TO LANDMINES DETECTION

V.Kovalenko, A.Yarovoy, L.P. Ligthart
Delft University of Technology, Mekelweg 4, Delft 2628CD, The Netherlands
V.Kovalenko@irctr.tudelft.nl A.Yarovoy@irctr.tudelft.nl L.P.Ligthart@irctr.tudelft.nl

1. Introduction

The humanitarian demining is one of the most challenging problems confronting mankind and significant efforts have been made to develop high-tech tools to solve the problem [1]. The GPR technology is considered as one of several promising technologies, which should be used to solve the problem [2]. The GPR provides a relatively cheap and safe way of the detection of abrupt changes in material parameters of the ground, which can be considered as a subsurface image.

The use of GPR technology for detecting antipersonnel landmines (APM) is dumped, however, by strong attenuation of the electromagnetic waves in the ground and presence of strong clutter caused by inhomogeneities of the soil. Much work has been done to improve both GPR hardware and data processing tools to overcome these problems. But despite significant advances in both directions, the problem of the clutter suppression still remains a most difficult one, especially when APM with low metal content are to be detected in highly inhomogeneous soil.

In this paper we consider statistical properties of 2-D maps, which result from processing 3-D GPR datasets. Use of the 2-D maps rather then full 3-D images is justified by demand of potential end-user of the equipment to have a map with suspicious spots marked. The high level of clutter often present in the processed subsurface image complicates the APM detection by means of threshold. This calls for statistical analysis of the images of clutter regions and mines. In this paper we present the distinctive statistical features peculiar to the mine image in our data and use them to discriminate the APM in the WEP map contaminated with clutter.

2. Hardware description and measurement setup

The data, which are used to produce the images under investigation, have been acquired with full polarimetric video impulse GPR [3] developed in IRCTR, TU Delft. The IRCTR GPR is specially designed for landmine detection and meets high stability requirements inherent to this type of applications. The radar emits short electromagnetic impulses with bandwidth from 0.5 till 3 GHz depending of the generator used. The pulses are emitted with 2 orthogonal transmit antennas and received with 4 independent receive antennas. Here we consider the data acquired in quasi-monostatic and bi-static co-polarized channels.

The measurements have been made at the test facilities for landmine detection systems located at TNO-FEL [4]. The data have been collected over the sand and the grass lane. The APM simulants have been placed on the surface of the lanes and on the depths of 1 and 6 cm (from the tops) in the sand and 0 and 5 cm in the grass. The simulants of PMN2, which is ~12 cm diameter and M14 (~6 cm diameter) APM were found in the sand. Both mines have low metal content. The simulants of PMN2, M14 and "Butterfly" mines are placed in the grass. The 'Butterfly" mine has assimetric shape of ~4 cm main diameter and contain significant amount of metal.

The radar was mounted on the relocatable frame, which allows accurate positioning of the radar in each moment of the measurements and stable movement over the spot being measured. The measured spots were the time-space cubes of the dimension of 10ns*256*240 cm^2. The heights of the receiving antennas over the surfaces were chosen to be 20 cm over the sand and 10 cm over the grass. The data resulting from the experiments are the C-Scans of dimensions 512*465*79 $samples^3$ acquired in regular but non-uniform grid: the distance between the adjacent A-Scans along the radar movement is 0.504 cm, while the distance between the adjacent B-Scans is 3 cm.

ISBN: 4-88552-206-4 C3055©IEICE

3. The data processing

The following 3-step processing scheme have been applied to the data:

1. Background removal by cylindrical moving window average subtraction
2. SAR focusing
3. 3D→2D mapping by Windowed Energy Projection (WEP)
4. Linear 2D interpolation of WEP map to obtain a uniform grid.

The background removal is realized by the following filter:

$$\widetilde{C}_{ij}(t) = C_{ij}(t) - \frac{1}{N} \sum_{\alpha x^2 + \beta y^2 \le 1} C_{xy}(t) \tag{1}$$

Where α and β define the ellipse, which is the section of the cylinder and N is the number of the A-Scans involved in each particular summation. The filter parameters were chosen here to form a circular cylinder with 20 cm radius in the physical space.

The focusing of the image is realized by means of the unweighted stack migration, which takes into account the ground-air interface and accounts for the ray bending.

The mapping of the 3-D volume image into surface is made by WEP rather than conventional energy projection. The latter is given by:

$$E_{ij} = \sqrt{\sum_{z=1}^{M} C^2{}_{z,ij}} \tag{2}$$

The output of (2) has simple physical meaning of the energy contained in each A-Scan of the migrated C-Scan. But due to natural clutter, imperfectness of the background removal by (1), artifacts of SAR algorithm itself, and other lateral effects the migrated C-Scan also contains sufficient amount of non-coherently distributed energy. This energy becomes the clutter in the EP map made according to (2).

The WEP is the tool of 3D→2D mapping, which is meant to preserve as much information of the object responses as possible, while leaving the incoherent energy behind. It utilizes the facts that the APM image in the migrated C-Scan is quite short (3 to 6 cm) and in our experiments there were no objects placed directly underneath each other. Taking this into account we can replace (2) with the following:

$$EW_{ij} = \max_{k} \left[\sqrt{\sum_{z=k-L}^{k+L} C^2{}_{ij}(z)} \right] \tag{3}$$

The procedure given by (3) represents each A-Scan of the migrated C-Scan not by its total energy, like in (2), but only by maximum energy level measured in the window of width L, which slides along the A-Scan. The choice of the window width is dictated by two contradicting factors: the window should include as much of the energy of the mine response as possible and be as narrow as possible to suppress the levels of the mine-free A-Scans. Finally, this should hold for all types of mines. As it can be seen from the Fig. 1, the growth of the energy for both types of mines found in the sand slows down after 3.8 cm. This value has been used ad the diameter of the window for the sand.

The WEP map has been linearly interpolated to produce the square-pixel image, which is shown in the Fig. 2. The homogeneity of the sandy lane and high quality of the raw data allow the detection of all the mines by simple threshold detector. This, in turn permits studying of the statistical properties of the mines and clutter regions in controlled conditions.

4. The statistical properties of the mine images and clutter regions

The first statistical parameter to describe is the histogram of the energy level distribution in the vicinity of the mine. Obviously, this parameter depends on the radius of the vicinity. The optimal choice of the radius would be the divisor of properties for vicinities of mine-less point and mine.

The energy distribution histogram for one of the PMN2 mines is given in the Fig. 3 a) for the different values of the vicinity radius. As it can be seen from the figure, the energy distribution for mine-containing vicinity is spread much wider than the mine-less one. We choose the radius of the vicinity equal to 7.4 cm as a compromise between the minimum radius, which provides statistical description for the bigger PMN2 mines and still doe not blur the statistical characteristics of the smaller M14 mines. For this fixed vicinity the Fig. 3 b) shows the histograms of the distribution of energy normalized on the value in the center of the vicinity for all the mines according to groundtruth (thin black

lines) and a mine-less region (thick gray line). The bold black line represents the mean of the histograms of the mines. As it can be seen from the figure, the energy distributions of all the mines is spread much widely in comparison with the mine-free region, regardless of the absolute values of the energy. Furthermore, the energy distribution of the clutter tends to normal one while even the weakest mines show more complex statistical behavior. This can be seen from the Fig. 4 a) where the normal plots for the mines and clutter are given. The significant difference in the standard deviation of the distributions, which defines the inclinations of the curves, is also noticeable. The estimation of interquartile range (IQR), which is a robust estimate of the data spread, is given on the Fig. 4 b) with use of mono- and bi- static channels of the radar. As it is shown in the figure, the linear division is possible. Even for the more complex WEP map (Fig. 5 a) of the grass lane the linear division of the IQR is possible with quite low amount of false alarms (Fig. 5 b).

5. Conclusion

We analyze the statistical properties of the high-resolution WEP maps of subsurface. We found that statistical distributions of the mine and clutter regions are essentially different. We have determined a number of distinctive features (such as a slope of the normal distribution plots and IQR), which may be used in a high performance statistical mine detector. We also demonstrated that simultaneous analysis of mono-static and bi-static images improves detectability of mines.

Acknowledgment

This research is supported by the Dutch Technology Foundation (STW) within the framework of the project "Advanced re-locatable multi-sensor system for buried landmine detection". The measurement campaign has been partly supported by TNO-FEL by providing free access to the test lanes.

Reference

1. The Demining Support System: Worldwide Analysis and Assessment - The International Union For Humanitarian Demining, 1999
2. A.G.Yarovoy "Advances in Ground Penetrating Radar for humanitarian demining", Proceedings of URSI-GA'02, XXVII General Assembly of the International Union of Radio Science, 2002
3. A.G. Yarovoy, L.P. Ligthart, A.D. Schukin, I.V. Kaploun., " Polarimetric Video Impulse Radar for Landmine Detection", *Subsurface Sensing Technologies and Applications*, vol.3, No.4, pp. 271-293, Oct. 2002.
4. Jong, W. de, Lensen H.A. and Janssen Y.H., "Sophisticated test facility to detect land mines", *Detection and Remediation Technologies for Mines and Minelike Targets IV*, *SPIE Proceedings*, vol. 3710, pp.1409-1418, 1999.

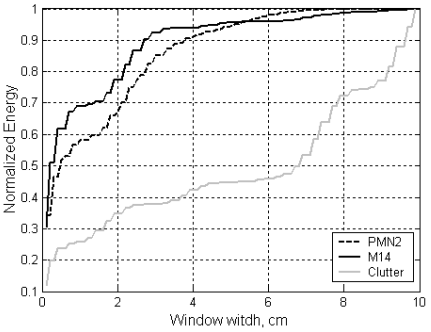

Fig. 1 Normalized energy content in window vs. window width for M14 (solid black), PMN2 (dotted) and mine-free A-Scan (gray).

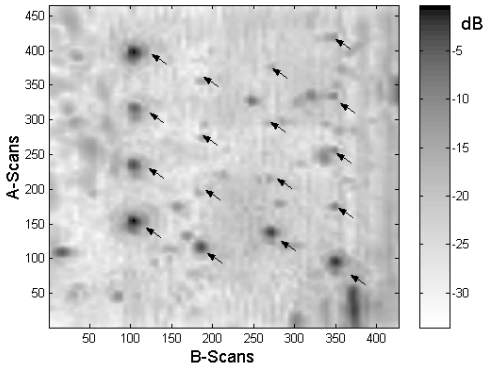

Fig. 2 The WEP map of the sandy lane. The mines depicted with arrows according to groundtruth

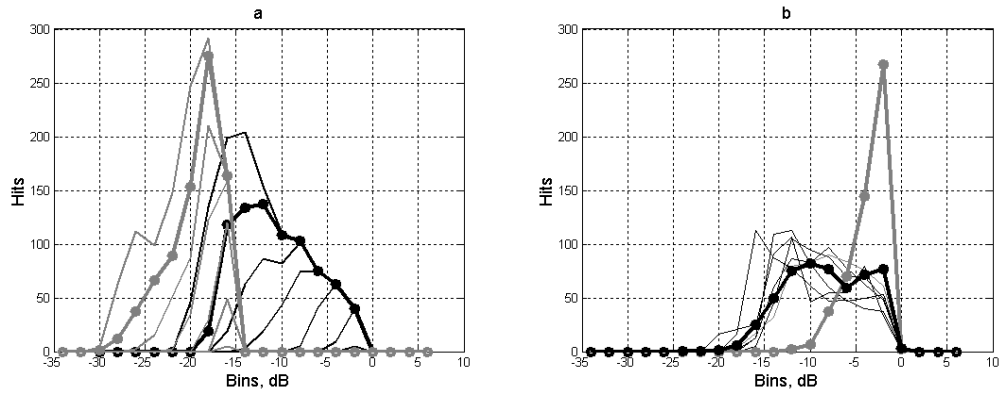

Fig. 3 a) Histograms of the energy distributions in the vicinity of a PMN2 mine (black) and clutter region (gray); the bold lines correspond to the r = 7.4 cm found to be optimal; b) histograms of the normalized energy distributions around mines (black) and clutter (gray); the bold black line is the mean of the histograms of all mines.

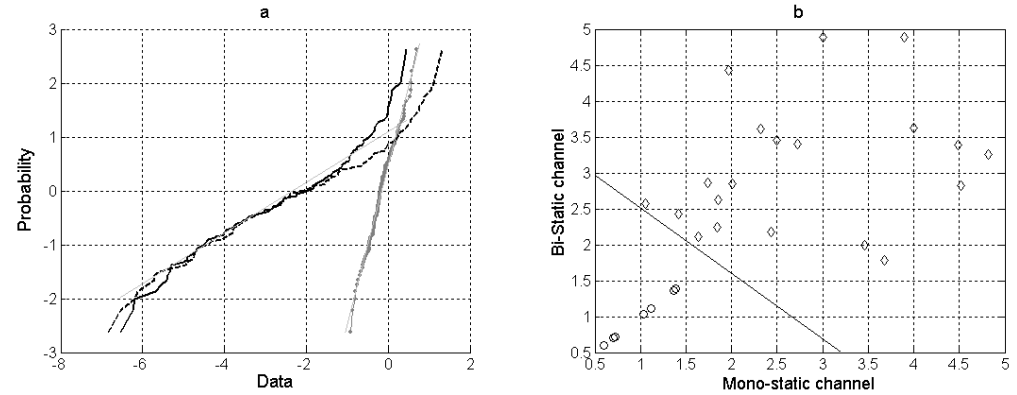

Fig. 4 a) Normal distribution plots for mines (gray) and clutter (black) b) Interquantile range of the energy distribution for mines (diamonds) and clutter (circles)

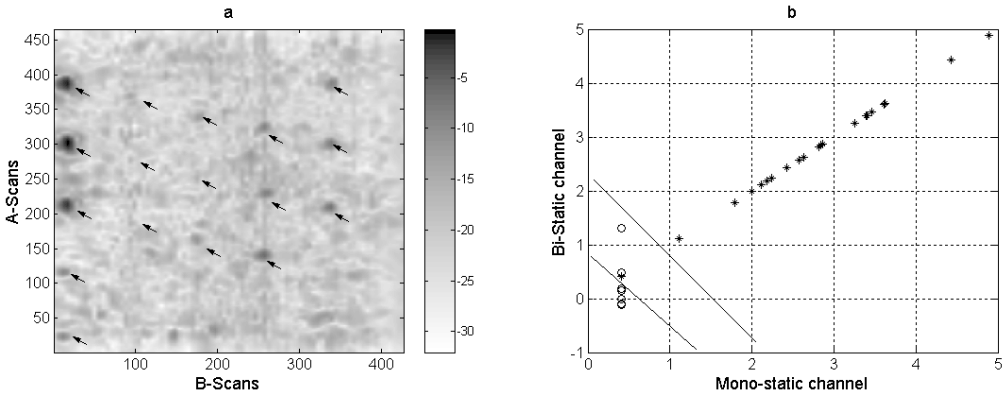

Fig. 5 a) The WEP map of the grass lane. The mines depicted with arrows according to groundtruth. b) Interquantile range of the energy distribution for mines (asterisks) and clutter (circles)